Slippery for scaling resistance in membrane distillation: a novel porous micropillared superhydrophobic surface

Zechun Xiao[1, 2], Rui Zheng[1, 2], Yongjie Liu[1, 3], Hailong He[3], Xiaofei Yuan[4], Yunhui Ji[5], Dongdong Li[1], Huabing Yin[4*], Yuebiao Zhang[3], Xue-Mei Li[1], Tao He[1,4 *]

[1]Shanghai Advanced Research Institute, Chinese Academy of Sciences, Shanghai 201210, China

[2]University of Chinese Academy of Sciences, Beijing 100049, China

[3]School of Physical Science and Technology, ShanghaiTech University, Shanghai 201210, China

[4]School of Engineering, University of Glasgow, Glasgow, G12 8LT, UK

[5]National Laboratory of Solid State Microstructures, Collaborative Innovation Center of Advanced Microstructures, College of Engineering and Applied Sciences, Department of Materials Science & Engineering, Nanjing University, Jiangsu, 210093, P. R. China

*Corresponding authors: het@sari.ac.cn, Tel: 0086-21-20325162, Fax: 0086-21-20320984

Abstract

Scaling in membrane distillation (MD) is a key issue in desalination of concentrated saline water, where the interface property between the membrane and the feed become critical. In this paper, a new slippery mechanism was explored as an innovative concept to understand the scaling behavior in membrane distillation for a soluble salt, NaCl. The investigation was based on a novel design of a superhydrophobic polyvinylidene fluoride (PVDF) membrane with micro-pillar arrays (MP-PVDF) using a micromolding phase separation (μPS) method. The membrane showed a contact angle of 166.0 ± 2.3° and the sliding angle of 15.8 ± 3.3°. After CF_4 plasma treatment, the resultant membrane (CF_4-MP-PVDF) showed a reduced sliding angle of 3.0°. In direct contact membrane distillation (DCMD), the CF_4-MP-PVDF membrane illustrated excellent anti-scaling in concentrating saturated NaCl feed. Characterization of the used membranes showed that scaling due to NaCl crystals and possible membrane wetting occurred on the control PVDF and MP-PVDF membranes, but not on the CF_4-MP-PVDF membrane. To understand this phenomenon, a "slippery" theory was introduced and correlated the sliding angle to the slippery surface of CF_4-MP-PVDF and its anti-scaling property. This work provides a well-defined physical and theoretical platform for investigating scaling problems in membrane distillation and beyond.

Keywords: micromolding phase separation; surface pattern; slippery; membrane distillation; scaling; membrane

1. Introduction

Highly saline wastewater streams from steel, chemical, petrochemical, and mining industries are of key concern for environmental and economical sustainability in developing countries (Latorre 2005, Shannon, Bohn et al. 2008, Bouchrit, Boubakri et al. 2015, Choi, Naidu et al. 2018, Deshmukh, Boo et al. 2018). Therefore, concentrating high salinity liquids has become an important task in water treatment. One of the main objectives in recent years is to concentrate close-to-saturation brine until zero-liquid-discharge (Yun, Ma et al. 2006, Shin and Sohn 2016, Junghyun, Heejung et al. 2017). Contemporary technologies, e.g. high pressure reverse osmosis (RO), electrodialysis (ED), mechanical vapor re-compression (MVR) and multi-effect distillation (Li, Wang et al. 2016) have been used, but all have different limitations. For example, RO and ED are powered by electricity, and are normally expensive. MVR and ED not only require high energy but also suffer from corrosion. Membrane distillation (MD) has attracted wide attention for desalinating highly concentrated brine with concentrations up to crystallization (Ji, Curcio et al. 2010, Nghiem, Hildinger et al. 2011, Edwie and Chung 2013, Chen, Lu et al. 2014, Hickenbottom and Cath 2014, Naidu, Jeong et al. 2014, Bouchrit, Boubakri et al. 2015, Chen, Wang et al. 2015, Tian, Yin et al. 2015, Eykens, Hitsov et al. 2016, Gryta 2016, Shin and Sohn 2016, Bouchrit, Boubakri et al. 2017, Chen, Tian et al. 2017, Chen, Zheng et al. 2017, Duong, Hai et al. 2017, Junghyun, Heejung et al. 2017, Choi, Naidu et al. 2018, Julian, Ye et al. 2018, Kim, Kim et al. 2018, Naidu, Zhong et al. 2018).

MD uses low grade heat or sustainable energy (such as solar power) and is potentially an affordable desalination technology (Alkhudhiri, Darwish et al. 2012, Tijing, Woo et al. 2015, Eykens, De Sitter et al. 2017). Normally, a MD system is compact, lightweight, and resistant to corrosion. However, similar to other membranes, MD membranes are prone to fouling, scaling and membrane

wetting (Tijing, Woo et al. 2015), which will lead to deteriorated performance. For high salt solutions, in particular when the concentration of salt approaches saturation, scaling becomes the most serious problem (Ji, Curcio et al. 2010, Gryta 2011, Edwie and Chung 2013, Chen, Lu et al. 2014, Hickenbottom and Cath 2014, Nariyoshi, Pantoja et al. 2016, Bouchrit, Boubakri et al. 2017, Jiang, Tuo et al. 2017, Tang, Iddya et al. 2017, Julian, Ye et al. 2018, Zou, Dong et al. 2018). Crystals attached to the membrane surface alter surface wettability (e.g. from hydrophobic to hydrophilic), allowing continuous crystal growth into membrane pores and consequently membrane wetting (Yun, Ma et al. 2006, Gryta 2008, Ramezanianpour and Sivakumar 2014). Wetted membranes result in free diffusion of salt molecules from the high salinity feed to the permeate, thus reducing membrane rejection. Although the consequence of scaling can be measured, the mechanism governing scaling is unknown. How to prevent scaling remains a significant challenge in membrane technology.

Observations of NaCl scaling have been reported in the literature. When treating 18 wt.% NaCl brine in direct contact membrane distillation (DCMD), a critical size of 25 μm was found for the crystals on the PVDF membrane surface, which acted as initial growth sites and led to the full membrane coverage (Chen, Lu et al. 2014). Single NaCl crystals of 40 μm were also reported in a membrane distillation-crystallization (MDC) process, where about 9 to16% of the total crystals were on the membrane surface and the piping (Nariyoshi, Pantoja et al. 2016). Scaling often occurred when the feed reached saturation (Bouchrit, Boubakri et al. 2015, Gryta 2016, Bouchrit, Boubakri et al. 2017). Injection of air (Choi, Choi et al. 2017) and increase of the feed flow velocity (Naidu, Jeong et al. 2014, Choi, Choi et al. 2017) can mitigate scaling. However, when optimization of process parameters such as flow rate and temperature reversal were used to mitigate rapid flux decline in concentrating salt lake brine, there was little successes (Hickenbottom and Cath 2014).

Instead of optimizing process parameters, membrane modification provides another important route to mitigate or prevent scaling. An electrically conducting membrane surface can be made by coating a carbon nanotube/poly(vinyl alcohol) (PVC) layer onto a polypropylene support, which can effectively dissolve silicate scale during desalination of geothermal brine (Tang, Iddya et al. 2017). It has been shown that air bubbles can be created on the superhydrophobic surface of a perfluorodecyl acrylate modified poly(vinyldene fluoride) PVDF membrane (i.e. via initiated chemical vapor deposition, iCVD), which can suppress MD fouling despite increased crystal formation (Warsinger, Servi et al. 2016). However, in another study, a superhydrophobic membrane prepared by coating TiO_2 nanoparticles on a PVDF electrospun nanofiber support followed by chemical fluorosilanization, promoted more uniform and slower crystal formation and removal of the crystal deposition was easy (Razmjou, Arifin et al. 2012, Meng, Ye et al. 2014, Meng, Ye et al. 2015).

The majority of research on superhydrophobic membranes are based on chemical modification and /or the design of hierarchical structure (Razmjou, Arifin et al. 2012, Wei, Zhao et al. 2012, Meng, Mansouri et al. 2014, Meng, Ye et al. 2014, Yang, Li et al. 2014, Meng, Ye et al. 2015, Tian, Yin et al. 2015, Yang, Tian et al. 2015, Lee, An et al. 2016, Tijing, Woo et al. 2016, Warsinger, Servi et al. 2016, Ren, Xia et al. 2017). Contradictory results were often observed (e.g. the examples above). These might be due to variations in the feed as well as undefined surface morphology. An intuitive assumption in MD is the existence of a static membrane/liquid interface. Therefore, it has been believed that mimicking the hierarchical structure of lotus leaves could provide an anti-fouling solution. However, actual fouling/scaling in MD occurs at triple-phase interfaces consisting of liquid phase (feed) – air phase (in pores) – solid phase (polymer). If the tri-phase interfaces are not always static, scaling can occur in different ways. The mechanisms underlying fouling and scaling in MD is highly complex.

105 To address this challenge, our vision is to design a simple, but structurally well-controlled membrane
106 surface that can modulate the interface properties and provide a dynamic contact line between the
107 membrane and water phase.

108 Advances in nanofabrication technology have been used to create superhydrophobic surfaces (Li,
109 Reinhoudt et al. 2007, Xue Mei Li 2007, Li, He et al. 2008) and surfaces with multidimensional
110 roughness (Kim, Lee et al. 2016). A recent study shows that MD membranes patterned with a groove
111 structure have a weak hydrophobic interaction with BSA proteins and hence low fouling propensity
112 (Xie, Luo et al. 2017). However, since the evaluation was in static conditions, information on scaling
113 was not available. Similarly, corrugated PVDF membranes demonstrate the ability to alleviate salt
114 deposition and fouling in DCMD of real seawater (Kharraz, Bilad et al. 2015), but the dynamics of
115 scaling was unknown.

116 Here, we attempt to understand the dynamic mechanisms of scaling at the liquid-air-solid interface
117 in MD. For the first time, a patterned superhydrophobic PVDF membrane with porous micropillars
118 was prepared via a micro-molding phase separation (μPS) technique. A similar technique has been
119 used to create macro-patterned surfaces for pressure driven membranes (Çulfaz, Rolevink et al. 2010,
120 Çulfaz, Haddad et al. 2011, Çulfaz, Wessling et al. 2011, Hashino, Katagiri et al. 2011, Won, Lee et al.
121 2012, Jamshidi Gohari, Lau et al. 2013, Lee, Won et al. 2013, Gençal, Durmaz et al. 2015, Maruf,
122 Greenberg et al. 2016, Won, Jung et al. 2016, ElSherbiny, Khalil et al. 2017). However, pressure driven
123 processes only involve a liquid-solid interface with a convective flow of liquid across the membrane.
124 Therefore, it is fundamentally different from the vapor diffusion-based MD process. Here, porous
125 micro-pillar formation together with CF_4 plasma treatment allowed the creation of a superhydrophobic
126 PVDF membrane, which is employed to investigate: (1) the relationship between the micro-pattern

and the hydrophobicity of the membrane surface; and (2) the relationship between the micro-pattern and the scaling property in DCMD for highly concentrated NaCl solutions. The superhydrophobic membrane demonstrated excellent anti-scaling properties when used to treat a saturated NaCl solution by DCMD. The results lend us to propose a "slippery surface" as a dynamic means of preventing scaling in MD. The novel multiscale hierarchical surface illustrated in this work also offers a promising platform for understanding and mitigating the scaling and fouling problems in other processes beyond MD.

2. **Materials and methods**

2.1 Materials and chemicals

PVDF (Solef 1015) was kindly supplied by Solvay. N, N-Dimethylacetamide (DMAc, AR) and Diethylene glycol (DEG, AR) were purchased from Sinopharm Chemical Reagent Co. Ltd and used without further purification. The silicon wafer mold with a pillar array was designed in house. The dimensions of the pillars are 5 μm in diameter (D), 10 μm in height (H) and 10 μm in period (P) (Fig.1). A commercial flat sheet polyvinylidene fluoride membrane (abbreviated as C-PVDF, GVHP, Millipore, USA) with a nominal pore size of 0.22 μm and thickness of 125 μm was used as a benchmark.

2.2 Fabrication of polydimethylsiloxane (PDMS) mold

Oligomer PDMS and the curing agent (SYLGARD 184, Dow Corning Co. Ltd) were pre-mixed at a weight ratio of 10:1. After de-gassing in vacuum for 10 min, the mixture was cast onto the silicon wafer template. Then the wafer and the PDMS solution was transferred into a vacuum oven and cured for 3 hours at 60°C. The PDMS replica was then peeled off and stored in a clean container. The entire

process was carried out in a clean room.

2.3 Fabrication of MP-PVDF membrane

A PVDF casting solution (PVDF/DEG/ DMAc, 15/27.4/57.6 wt.%) was prepared by mixing the components in a flask at 90 °C and agitated for 12 h. The polymer solution was then filtered using a metal filter of 40 µm. The casting solution was kept at 90 °C to de-gas. Fig. 1 shows the procedure for the fabrication of micro-pillar PVDF membranes and details are as follows.

An appropriate amount of the PVDF solution was spread uniformly on the PDMS replica on top of a glass plate to a thickness of 600 µm using a home-made stainless-steel casting knife. The solution was exposed to water vapor for 10 s (10 cm above a coagulation water bath, 75°C) and then immersed in the coagulation bath for 15 minutes to induce precipitation. Upon precipitation, the membrane delaminated from the replica spontaneously. After rinsing with water to remove solvent and additives, ethanol was used to rinse the membrane before being dried in a vacuum oven at ambient temperature for 48 h. The resultant membrane is denoted as micro-pillared PVDF membrane (MP-PVDF).

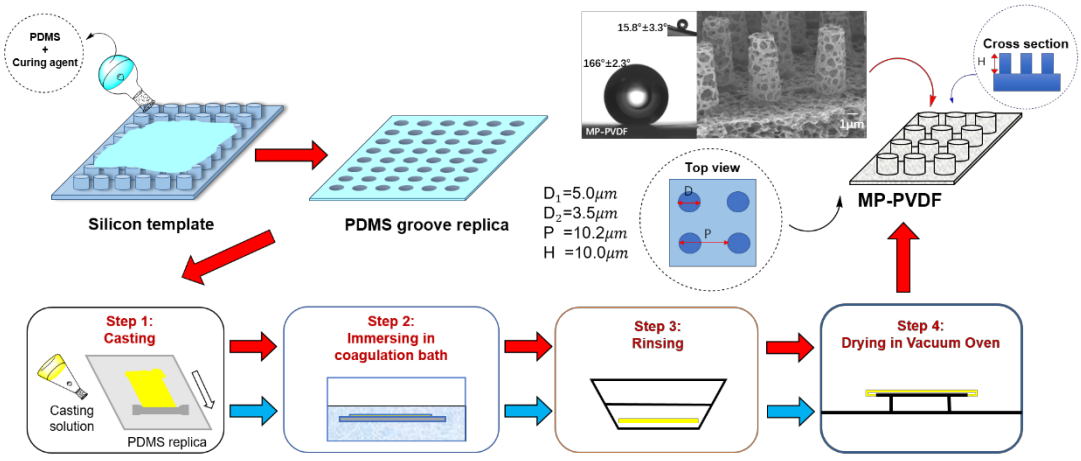

Fig. 1 Schematic for the fabrication of micro-pillar PVDF membranes (MP-PVDF). The silicon wafer mold has pillars with the dimension of 5 µm (diameter), 10 µm (height) and 10 µm (period).

167

168 2.4 Membrane modification by CF_4 plasma treatment

169 MP-PVDF membrane was further treated with CF_4 plasma (an IoN40 plasma system, PVA Tepla
170 Co.Ltd) to improve its hydrophobicity based on our previous methods (Wei, Zhao et al. 2012, Yang,
171 Li et al. 2014, Yang, Tian et al. 2015, Chen, Tian et al. 2017, Chen, Zheng et al. 2017). In brief, the
172 substrate was cleaned first under argon plasma at 45W for 15s and then in CF_4 gas at a flow rate of
173 120 cm^3/min (SCCM) at 200W for 15 min. After the CF_4 modification, the chamber was cleaned using
174 an O_2 plasma at 200W for 15 min to avoid any CF_4 deposition on the electrodes.

175 2.5 Membrane characterization

176 Water contact angle (CA) and sliding angle (SA) of the samples were measured using a contact
177 angle goniometer (Maist Drop Meter A-100P) via the sessile drop method. The tilt angle at which the
178 droplet started rolling off the surface was denoted as the sliding angle. Pore size and pore size
179 distribution were analyzed using porometry (Porolux 1000, Supplementary information Method S1)
180 (Wei, Zhao et al. 2012, Yang, Li et al. 2014, Yang, Tian et al. 2015, Chen, Tian et al. 2017, Chen,
181 Zheng et al. 2017). Scanning electron microscopy (HITACH TM-1000 and FEI Nova Nano SEM 450)
182 was used to characterize membrane morphology. The sample was sputtered with a thin layer of gold
183 in a vacuum prior to SEM characterization.

184 2.6 MD performance

185 A bench scale DCMD unit (Supplementary Data Fig. S1) developed previously (Wei, Zhao et al.
186 2012, Yang, Li et al. 2014, Yang, Tian et al. 2015, Chen, Tian et al. 2017, Chen, Zheng et al. 2017)
187 was used to evaluate scaling on the membranes using 4 wt.% or 25 wt.% NaCl solutions. For the MP-
188 PVDF and CF_4-MP-PVDF membranes, the side with pillars was in contact with the feed. The

conductivity of the permeate was regularly measured to identify the point when salts from the feed penetrate to the permeate. Since 25 wt.% is close to the saturated concentration for a NaCl solution, the experimental duration was significantly reduced. The feed and the permeate temperatures were maintained at 60 ± 0.3 °C and 20 ± 0.3 °C respectively. The flux (J, kg/m^2·h) was calculated based on equation (1):

$$J = \Delta m / A \Delta t. \qquad \text{Equation (1)}$$

Where Δm (kg) is the amount of water transported from the feed to the permeate, Δt the interval of the collection (h) and A the membrane area (m^2).

3. Results and discussion

3.1 Morphology of the MP-PVDF membrane

Fig. 2 shows the SEM images of the top, bottom and cross-section of the commercial PVDF (C-PVDF) and micro-pillar PVDF (MP-PVDF) membrane. Both membranes show a porous top and bottom surface, as well as a macroporous cross-section. The surface porosity and pore size of MP-PVDF membranes appears to be lower than C-PVDF membranes. In addition, MP-PVDF membranes contain porous pillar arrays with open structure throughout (Fig. 2, inserts). For the sake of clarity, the membrane surface facing the feed is denoted as the top surface. In this study, the top surface of the MP-PVDF membrane (Fig. 2) was the one in contact with the PDMS replica. During membrane formation, phase separation started from the open surface of the polymer solution; instantaneous demixing occurred at the water/polymer solution interface, resulting in a finger-like macrovoid structure (i.e. MP-PVDF cross-section in Fig. 2). However, solvent and additives from the polymer solution within the PDMS replica had to diffuse through the whole membrane to the water bath and

211 therefore it was a slow process. This allowed the polymer-lean phases to grow and eventually enlarge
212 into micropores (He, Mulder et al. 2003, Li, Ji et al. 2008, Ji, Li et al. 2010, Li, Ji et al. 2010). The
213 interconnected porous structure in the top surface of the PVDF membrane is due to the competition
214 between the solid-liquid phase separation and liquid-liquid separation for a semi-crystalline polymer
215 (Xing, Song et al. 2016). The open porous surface in the pillars is of particular interest for creating a
216 superhydrophobic surface.

217 The MP-PVDF membrane features an array of conical pillars of 5 μm at the bottom (i.e. the part
218 connected to the bulk membrane) and 3.5 μm at the tip. Compared to the original pillar structure on
219 the silicon mold, this reduction at the tip is likely caused by membrane shrinkage during phase
220 separation. Nevertheless, the height and period for pillars on the membrane are the same as the
221 designed silicon mold, i.e. 10 μm in both height and period.

222

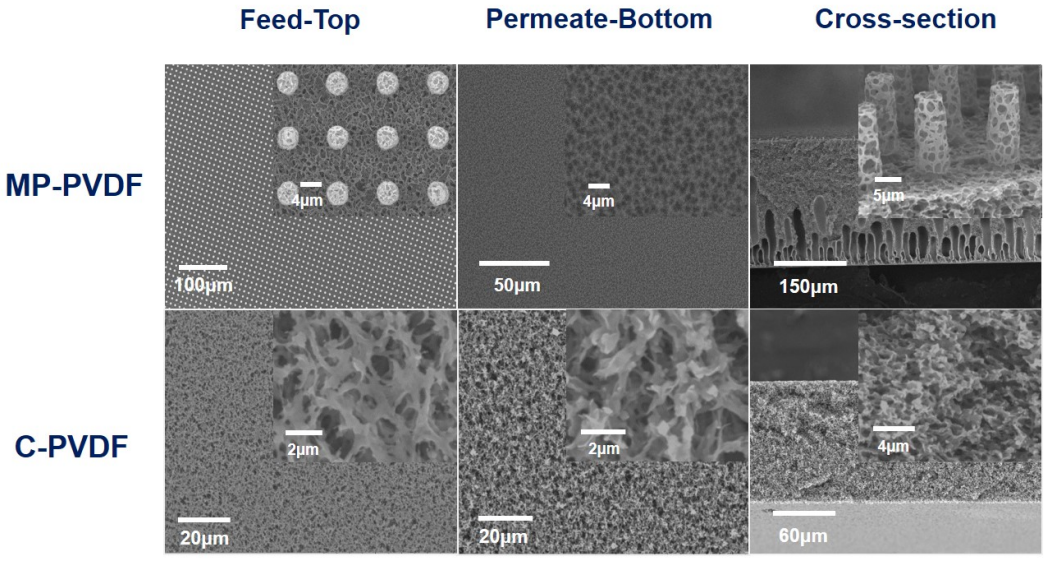

223

224 Fig. 2 SEM images of MP-PVDF and C-PVDF membranes. Feed-Top, Permeate-bottom and cross
225 section. The top surface of MP-PVDF was slight tilted for a better view. Inserts are enlarged views.

226

As listed in Table 1, the MP-PVDF membrane has a thickness of ~264 μm, whereas the commercial PVDF membrane (C-PVDF) is of 130 μm. Attempts to reduce this thickness could be possible by controlling the casting process. Slightly higher porosity is found in MP-PVDF membranes (~79 %) than C-PVDF membrane (75 %), indicating a more open porous substrate in MP-PVDF. However, the mean pore size of MP-PVDF membranes (0.120 μm) is smaller than C-PVDF membranes (0.230 μm). Interestingly, the contact angle for MP-PVDF membranes (166.0±2.3°) is significantly higher than that of C-PVDF membranes (139.2±3.7°). The CF_4 plasma treatment may fluorinate membrane surfaces by F atom insertion or deposition of Teflon polymers (Yang, Li et al. 2014, Tian, Yin et al. 2015, Yang, Tian et al. 2015). This leads to a slightly enlarged mean pore size (i.e. from 0.120 μm to 0.201 μm), and further increased contact angle (i.e. from 166° to 176°). As shown in FigS2. (Supplementary Data) , C-PVDF membrane possessed a narrow distribution of pore size, whereas C-PVDF and CF_4-MP-PVDF showed a relatively large pore size distribution.

The most striking difference is the sliding angle: C-PVDF membranes showed no sliding angle below 90°; MP-PVDF membranes showed a sliding angle of 15.8°; and CF_4-MP-PVDF showed a sliding angle of only 3.0°. The surface of CF_4-MP-PVDF membrane was so water repellent that a water droplet stuck to the needle rather than the membrane surface during the contact angle test. When the water droplet was released from the needle by a gentle flick, it rolled off the surface upon slight tilting. The surface energy follows a reverse order compared to the contact angle: C-PVDF membrane show the highest surface energy of 72 mJ/m^2, and CF_4-MP-PVDF membranes show the lowest energy of 0.27 mJ/cm^2. This water repelling property and low surface energy of the CF_4-MP-PVDF membrane surface are not trivial characteristics, which are most probably related to the scaling/fouling process as shown in the experiments below.

Table 1. Characteristics of the C-PVDF, MP-PVDF and CF_4-MP-PVDF membranes.

Membrane	C-PVDF	MP-PVDF	CF_4-MP-PVDF
Thickness/ μm	132 ± 3	263 ± 2	264 ± 2
Mean pore size/ μm	0.230 ± 0.0020.235±0.013	0.078 ± 0.0120.120±0.005	0.073 ± 0.0090.201±0.013
Porosity (%)	75.3±2.1	79.6±3.7	78.9±5.3
Contact angle/^{o}	139.2±3.7	166.0±2.3	175.6±1.3
Sliding angle /^{o}	>90	15.8±3.3	3.0±0.8
Surface energy (mJ/m^2)*	71.8±2.4	47.3±0.6	0.27±0.12

* Supplementary information Method S2 for determination of surface energy.

Both MP-PVDF and CF_4-MP-PVDF membranes can be categorized as superhydrophobic due to their high contact angle and low sliding angles. The commercial PVDF membrane has a very open porous surface, but its contact angle was only 139°, and its sliding angle is above 90°. Water droplets on a hydrophobic surface are normally considered as either in the Cassie-Baxter state or in the Wenzel state (Li, Reinhoudt et al. 2007, Xue Mei Li 2007, Li, He et al. 2008, Tian, Li et al. 2015). The difference between the two states is the contact areas between the water and the solid substrate: The Wenzel state is characterized by a larger contact area and more interaction between the liquid phase and solid phase, whereas air pockets between the liquid and solid phase are expected for the Cassie-Baxter state. Sliding angle is an indirect macroscopic feature indicating interaction between a surface

and a water droplet. A sliding angle above 90°, is an indication of strong interaction between the surface and water. This minor, but very important information shows that the surface characteristics of the C-PVDF membrane is different from that of micropillared membrane (MP-VPDF and CF_4-MP-PVDF). For C-PVDF membranes, the water contact angle was found to be much higher than 90°, and no obvious wetting upon immersion in water was observed. However, if comparing to MP-PVDF and CF_4-MP-PVDF membranes with a high contact angle and low sliding angle, it is likely that water on C-PVDF surface is in a meta-Cassie-Baxter state with partial wetting. The cause might be related to the surface morphology: C-PVDF membrane has a homogeneous porous surface, but both MP-PVDF and CF_4-MP-PVDF have pillars with higher surface porosity. The state of water in contact with the membrane surface is not clear yet at this stage, but worthy of future analysis. Previous work on MD membranes with a superhydrophobic or omniphobic surface only considered static water contact angles, and did not measure sliding angles (Wei, Zhao et al. 2012, Lin, Nejati et al. 2014, Yang, Li et al. 2014, Nejati, Boo et al. 2015, Tian, Yin et al. 2015, Yang, Tian et al. 2015, Boo, Lee et al. 2016, Boo, Lee et al. 2016, Lee, Choi et al. 2016, Lee, An et al. 2016, Lee, Boo et al. 2016, Tijing, Woo et al. 2016, Wang, Hou et al. 2016, Wang, Jin et al. 2016, Chen, Tian et al. 2017, Chen, Zheng et al. 2017). In the MD process, water flows along the membrane surface, and thus behaves dynamically. Increasing the feed flow rate was reported to mitigate scaling (Naidu, Jeong et al. 2014, Choi, Choi et al. 2017), which might be relevant to the dynamic behavior at the interface between water and membrane.

283 3.2 MD performance

284 Fig. 3 shows the flux and permeate conductivity using C-PVDF, MP-PVDF and CF_4-MP-PVDF
285 membranes. An initial feed solution of 25 wt.% NaCl was concentrated until changes in the flux or
286 permeate conductivity occurred. We intentionally selected this close-to-saturation concentration to
287 reduce the experiment time. With increased concentration, the C-PVDF membrane showed a gradual
288 decrease in flux. When the concentration factor (i.e. the ratio of the salt concentration during the
289 process to its initial concentration in the feed) reached about 1.1, the flux suddenly dropped to zero. A
290 similar trend was found for the MP-PVDF membrane, but at a concentration factor of about 1.2. In
291 contrast, CF_4-MP-PVDF membranes maintained a surprisingly stable flux at much higher
292 concentration factors (i.e. 1.76). Initial tests using a 4 wt.% NaCl feed solution showed no obvious
293 variations in both flux and permeate conductivity for the three membranes. They were intact and
294 remained integral (Supplementary information, Fig. S3). Reproducibility of the DCMD results was
295 confirmed as shown in Supplementary Data, Fig. S4.

296 In terms of flux, CF_4-MP-PVDF showed a slightly higher initial flux than MP-PVDF. This is
297 probably due to the enlarged effective evaporation surface area at the liquid-air-solid interface which
298 contributed to the increased water flux (Yang, Li et al. 2014, Yang, Tian et al. 2015). This difference
299 gradually disappeared when the concentration factor reached 1.1, and after that both CF_4-MP-PVDF
300 and MP-PVDF membranes showed a similar flux.

301 In the case of permeate conductivity, very different results were obtained (Fig. 3B). The permeate
302 conductivity of C-PVDF membranes increased gradually until a concentration factor of 1.1 (i.e. the
303 flux declined to zero). Similar trend was observed for MP-PVDF membranes. For CF_4-MP-PVDF, the
304 permeate conductivity increased continuously throughout the whole process until 350 μS/cm, without

obvious sacrificing in MD flux. This phenomenon is striking in that saturated NaCl feed would generally cause instantaneously scaling and dramatic flux decline in MD (Tun, Fane et al. 2005, Gryta 2010, He, Gilron et al. 2013). Increase in permeate conductivity is an indication of diffusion of NaCl from saturated feed to the permeate; however, at the concentration factor of 1.76, the CF_4-MP-PVDF membrane showed a rejection of 99.9% (Supplementary Data Fig. S5). Although this value is very high, rigorous analysis would claim that current membrane is not perfect or other unknown mechanism exists. For CF_4-MP-PVDF, the permeate conductivity increased continuously throughout the whole process until 350 μS/cm, without obvious sacrificing in MD flux. Minor defects in the membrane allow diffusion of NaCl from feed to permeate; at low feed NaCl concentration, the diffusion of NaCl is minor thus the permeate conductivity does not show appreciable increase; but at saturation, diffusion of NaCl is noticed in the permeate. Besides the contribution of defects, the other contribution might be the NaCl aerosol generated at the interface from the saturated feed eventually pass the porous hydrophobic pores and end in the permeate. Sea salt aerosol (SSA) has been routinely found at the marine boundary(Tyree, Hellion et al. 2007, Jentzsch, Ciobotă et al. 2011). We have to admit that this hypothesis is of no direct proof yet and requires further scientific investigation.

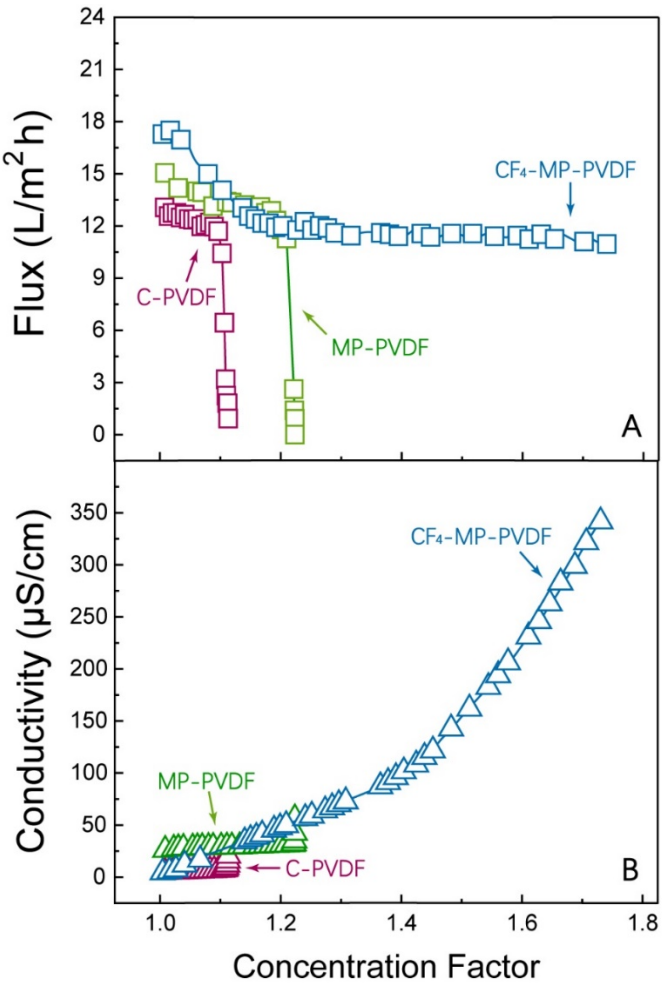

Fig. 3 DCMD performances of C-PVDF, MP-PVDF and CF_4-MP-PVDF membranes with an initial 25wt. % NaCl feed solution. A and B: Water flux and permeate conductivity of three membranes as a function of concentration factor. The feed temperature was maintained at 60 °C and the permeate temperature at 20 °C. The concentration factor is defined as the ratio of the salt concentration in the feed during the process to the initial salt concentration (i.e. 25 wt.% NaCl).

After the DCMD experiment, membrane samples were removed from the test cell and characterized as shown in Fig. 4. The contact angle for both C-PVDF and MP-PVDF membranes, was significantly reduced. The sliding angle of MP-PVDF membranes increased dramatically from 15.8° to above 90°, indicating that the surfaces became sticky to water. In contrast, the contact angle of CF_4-

MP-PVDF membranes remained unchanged, but the sliding angle slightly increased from 3.3° to 10.5°. Optical images showed that the surfaces of CF_4-MP-PVDF on both feed and permeate sides remained clean. However, the surfaces of both C-PVDF and MP-PVDF membranes showed NaCl crystals (as highlighted by the red circles in Supplementary Data Fig. S6). This observation was further confirmed by the SEM images (Fig. 4B): a layer of NaCl crystals of various sizes were observed on the C-PVDF surface and some cubic crystals even imbedded in the middle of the support; furthermore, even permeate surface showed some cubic particulates which would be NaCl crystals. The surface of MP-PVDF was fully covered by a thick layer of NaCl crystals, and no full-sized pillars could be identified, no obvious large NaCl crystals were found in the porous structure.

Obviously, the scaling behavior of three membranes in concentrating the NaCl solution was different, caused by the different membrane morphology and chemistry. A large thick layer of crystals on MP-PVDF membrane indicates that the NaCl was mainly at the membrane surface (and in the original open space between pillars), but for C-PVDF membranes, liquid might have penetrated into the support; or C-PVDF membrane was partially wetted. In MD process, external concentration polarization and temperature polarization tend to increase the possibility of NaCl nucleation at the membrane surface(Schofield, Fane et al. 1987, Martínez-Díez and Vázquez-González 1999, Yang, Tian et al. 2015). Consequently, at a concentration factor of 1.1, the feed bulk reached salt concentration above the saturation point (Godoy, Carvalho et al. 2017); at the same time, the salt concentration at the membrane/liquid interface is even higher than the bulk. It is thus probable that the nucleation of NaCl occurs at membrane surface before in the bulk. Therefore, the scaling for both C-PVDF and MP-PVDF membranes is initiated from the surface rather than in from the bulk feed. Difference in the extend of scaling for C-PVDF and MP-PVDF membranes could be resulted from the

different surface morphology. The micropillars in the MP-PVDF membranes surface tend to create micro turbulence(Lee, Won et al. 2013, Jung, Won et al. 2015, Won, Jung et al. 2016); the thick crystal layer is most probably originated from this turbulence which lead to quick nucleation of NaCl crystals, thus coverage of the membrane surface. However, C-PVDF membrane has rather homogeneous surface pores; nucleation of NaCl crystals lead to wetting, resulted in crystals in the support layer. This phenomenon has been reported and nucleation and wetting of the polypropylene membranes by NaCl concentrated solution. As a consequence, the MD flux declined as soon as the membrane was wetted(Gryta 2002, Gryta 2002).

Very interesting observation was that CF_4-MP-PVDF membrane did not show any scaling or fouling, and the MD flux was very stable at a concentration factor of 1.78, far above the saturation. Assuming that the feel did not form NaCl crystals in the bulk, the solution was then super-saturated. Although supersaturation without crystallization is possible (He, Sirkar et al. 2009, He, Sirkar et al. 2009), one would expect that the vapor pressure of the supersaturated solution decreases; consequently, the MD flux would gradually decline. Therefore, the stable MD flux was an indication of constant feed NaCl concentration. This means that there probably was crystallization of NaCl from the feed solution after the solution was supersaturated. However, no suspension was observed in the bulk feed caused by the crystallization of NaCl in the experiment. The phenomenon will be further addressed in the next session. To unravel this puzzle is scientifically interesting and challenging, at present, we are not able to identify the origin of scalant yet. An online monitoring method will be required and the effect of the membrane surface morphology and chemistry on the scaling formation will be clarified and published in the future.

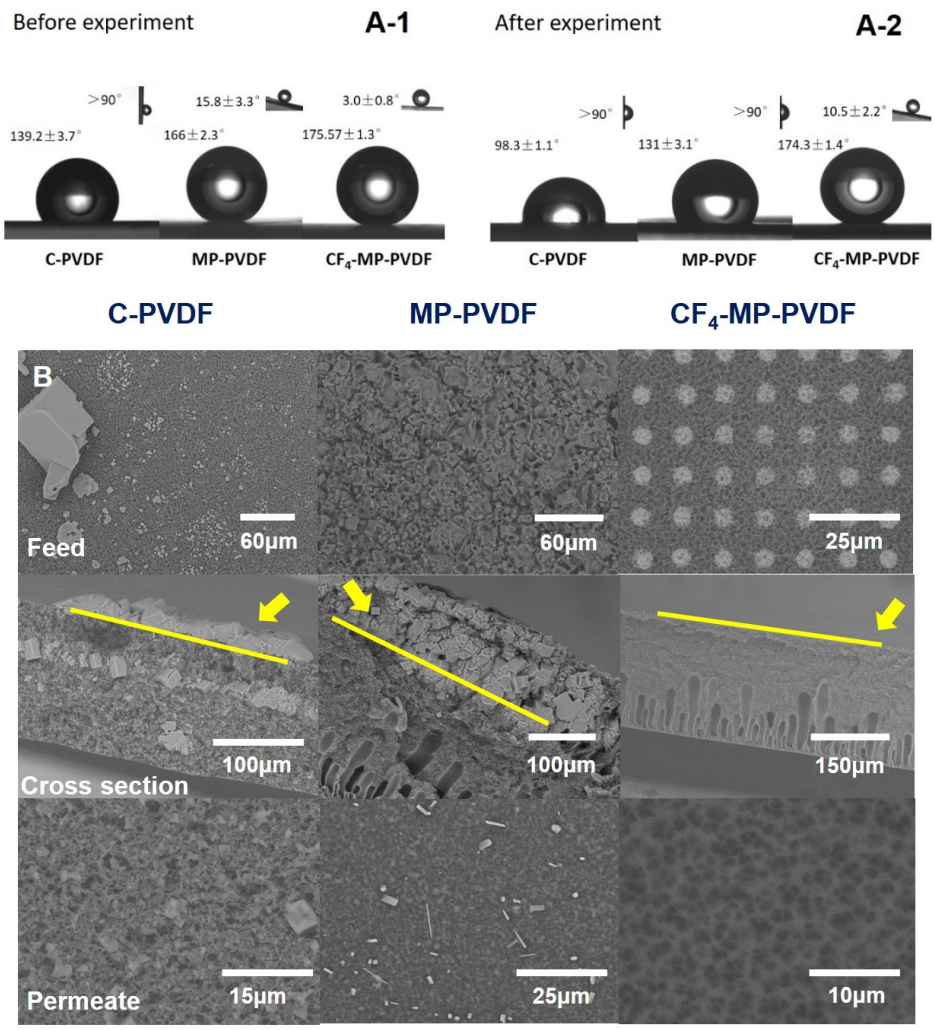

Fig. 4 Characteristics of C-PVDF, MP-PVDF and CF_4-MP-PVDF membranes before and after DCMD test. (A-1) and (A-2): contact angles and sliding angles of three membranes before and after DCMD; (B): SEM images of the surfaces and cross-section. For the cross-section images, arrows and lines indicate the membrane surface at the feed side. C-PVDF and MP-PVDF membranes showed aggregates of crystals.

3.3 Origin of anti-scaling: hypothesis

The reduction in the contact angle is obviously caused by the scaling by NaCl. Upon saturation, C-PVDF was scaled by NaCl crystals, followed by a rapid flux decline to zero. Although the MP-

PVDF membrane showed a delay to a concentration factor of 1.2, scaling was inevitable (Fig. 3 and Fig. 4 B). With such a harsh saturated solution, the clean surface of CF_4-MP-PVDF on the feed side demonstrated a surprising anti-scaling property. CF_4-MP-PVDF membranes have a very low sliding angle (Fig. 4 A-1), and their surface was repellent to water droplets. Correlation between the two phenomena raised questions: Did the water "feel" slippery at the liquid-air-polymer interface? Did this prevent the attachment of nucleation of NaCl crystals or attachment of crystals to the interface, leading to the CF_4-MP-PVDF membranes being resistant to scalant even in a supersaturated solution?

In our research, however, the results of the contact angle and sliding angle have already given hints on the dynamic behavior in MD. We utilized a peristaltic pump in the experiment to give extra force to increase the release of the matters from the membrane surface for reduction of scaling. Special care was taken to prevent bulky amount of air flow into the system; but sporadically some bubbles could be visualized to enter the module. As shown in Video S1 (Supplementary information), interesting phenomena on membrane surfaces in the feed were observed: (1) for MP-PVDF membrane, bubbles were constantly seen, slowly moving along the surface in the direction of the flow; (2) for C-PVDF membrane, bubbles were seen, but mostly remaining in place; sporadically some small air bubble flowing into the module moved along the flow; (3) for CF_4-MP-PVDF membranes (the video was modified into slow motion for a clear view), there were bubbles which appeared and disappeared constantly following the pulses of the pump; moreover, a large motion of liquid-air interface was observed along the membrane surface. Above difference, though preliminary and qualitative, enlightens us on an important factor for scaling resistance for CF_4-MP-PVDF membrane.

Hereby, we propose a hypothesis that the dynamics at the liquid-air-polymer interface largely

410 dictate scaling. We first define a “stick” or “slippery” surface based on sliding angle. C-PVDF was
411 defined as a “sticky” surface since its sliding angle is above 90° (Fig. 4 A-1). This “sticky” surface
412 might cause non-slip of the liquid phase at the interface. For a superhydrophobic surface with a very
413 low sliding angle, CF_4-MP-PVDF is defined as a “slippery” surface since its sliding angle is far below
414 10° (Fig. 4 A-1). This means that water actually “floats” above the air-polymer surface. For MP-
415 PVDF membranes, the magnitude of stickiness or slipperiness lies between the two extremes.
416 Slippery surface (SLIPs) with liquid infusion has been reported for inhibition of ice nucleation
417 or anti-ice/anti-frost performance(Kim, Wong et al. 2012, Kim, Kreder et al. 2013, Wilson, Lu et al.
418 2013). The slippery surface we proposed could be identified as “an air/vapor infused surface”. This
419 logic deduction would lead to similar concept of anti-scaling for NaCl crystals. This engineered
420 slippery liquid/air/solid interface is theoretically resistant to any crystalline particulates. We admit
421 that the effect of the chemistry nature and nucleation/growth of the crystals to scaling for
422 micropillared membrane is unknown and worth of further investigation. Because MD involves mass
423 transfer, concentration and temperature polarization, it is much more complicated than the SLIPs
424 surface created by liquid infusion(Kim, Wong et al. 2012, Kim, Kreder et al. 2013, Wilson, Lu et al.
425 2013). At present, we are conducting non-intrusive observation the formation of scaling and evidence
426 will be reported in the near future (Fortunato, Jang et al. 2018, Lee, Jang et al. 2018).
427 Consequently, a slippery surface is hypothesized to be scaling resistant because dynamically the
428 liquid remains floating above the polymer phase; or the fluid solid interface is constantly changing;
429 in other words, the liquid feels slippery at the interface. The observation of a large air/liquid interface
430 flowing along the membrane surface was an indirect proof. However, the direct consequence is that,
431 no crystals directly contact the polymer phase even though there are NaCl crystals in the liquid phase.

Thus, the chance for scaling is low (Fig. 5). For CF_4-MP-PVDF membrane, due to the constantly moving interface, very limited interaction of the liquid and the membrane polymer could not allow the formation of nuclei on the membrane surface; even if the solution contains crystals, it is also very difficult to attach to the surface. On the contrary, for a "sticky" surface, there exists a rather static liquid-air-polymer interface; above saturation, the chance for nucleation and growth on the membrane surface increases; Driven by the concentration and temperature polarization, NaCl crystals would form on the surface and so does scaling. The in-situ observation of the dynamic scaling process at the interface remains challenging. We are currently working with other scientists using optical coherence tomography (OCT) (Fortunato, Jang et al. 2018, Lee, Jang et al. 2018) to further confirm the observation and compare different surface morphology on the scaling for various inorganic salts.

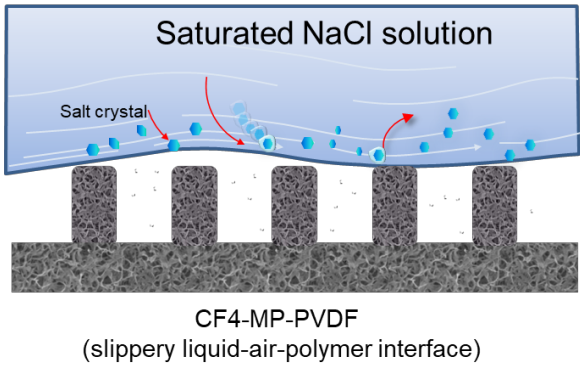

Fig. 5 Schematic of the slippery interface in relation to anti-scaling for CF_4-MP-PVDF membrane.

The other quantitative measure of the slipperiness of hydrophobic soft polymeric membrane surfaces has not yet been established in the literature. Nevertheless, the measurement of slipperiness of superhydrophobic surface has been reported as the slip length based on Navier's model (Granick, Zhu et al. 2003, Choi, Ulmanella et al. 2006). Measurement of the slip length of a surface would

indirectly support the present correlation of slip and scaling. Beyond scaling, the investigation of current slippery surface is useful for quantifying the flow resistance of the inner surface of a channel (Choi, Ulmanella et al. 2006, Truesdell, Mammoli et al. 2006, Daniello, Waterhouse et al. 2009, Haase, Wood et al. 2016). Low friction has been shown at a nanopatterned surface (Cottin-Bizonne, Barrat et al. 2003), which might be related to the formation of "nanobubbles" that gave rise to reduced friction resulting in a slippery surface (Tyrrell and Attard 2001, Shin, Park et al. 2015). As shown in video S1 (Supplementary information), we didn't observe nanobubbles, but a moving air/liquid interface along the superhydrophobic CF_4-MP-PVDF membrane surface. This observation provided a qualitative proof of the possible slippery character at the interface. Yet, the scientific evidence requires further experimental verification of the slip length and simulation of the flow pattern. The fundamental dynamic mechanism of scaling in membrane distillation could then be clarified. Understanding the dynamic scaling resistance might also shed light on fouling by other organic matter. This assumption lies in the probability of interaction between the foulant (in the feed) and the membrane materials. If direct contact between the membrane materials and the feed fouling is largely suppressed, fouling resistance might be observed.

4. Conclusion remarks

Superhydrophobic polyvinylidene fluoride (PVDF) membranes with micropillar arrays (MP-PVDF) were created via a micromolding phase separation (μPS) technology, providing a simple method for creating well-controlled surface morphology. With an additional CF_4 plasma treatment of MP-PVDF, the resultant CF_4-MP-PVDF had a significantly increased contact angle (174^o) and

471 decreased sliding angle (3.0°). This CF_4-MP-PVDF membrane showed less scaling upon concentrating
472 highly saline NaCl solution (25 wt.%) by direct contact membrane distillation. In contrast, both
473 commercial PVDF and MP-PVDF membranes showed severe scaling followed by flux reduction.
474 Membrane autopsy showed that scaling by NaCl crystals and possible wetting occurred in C-PVDF
475 and MP-PVDF, but not CF_4-MP-PVDF membranes. Visual observation of a floating water/air interface
476 in CF_4-MP-PVDF membranes qualitatively demonstrated that a slippery surface might contribute to
477 resistance to scaling. We hypothetically correlate the sliding angle to the slippery surface of CF_4-MP-
478 PVDF and its anti-scaling properties. This work may provide a platform and methodology for
479 understanding scaling beyond membrane distillation.

480 **5. Acknowledgements**

481 The research is supported by Newton Advanced Fellowship (Grant No. NA170113) and National
482 Natural Science Foundation of China (No. U1507117, 21676290). Zechun Xiao and Rui Zheng
483 contributed equally to the experimental work.

484 **6. References**

485 Alkhudhiri, A., N. Darwish and N. Hilal (2012). "Membrane distillation: A comprehensive review."
486 Desalination **287**: 2-18.
487 Boo, C., J. Lee and M. Elimelech (2016). "Engineering Surface Energy and Nanostructure of
488 Microporous Films for Expanded Membrane Distillation Applications." Environmental Science &
489 Technology **50**(15): 8112-8119.
490 Boo, C., J. Lee and M. Elimelech (2016). "Omniphobic Polyvinylidene Fluoride (PVDF) Membrane
491 for Desalination of Shale Gas Produced Water by Membrane Distillation." Environ Sci Technol
492 **50**(22): 12275-12282.
493 Bouchrit, R., A. Boubakri, A. Hafiane and S. A.-T. Bouguecha (2015). "Direct contact membrane
494 distillation: Capability to treat hyper-saline solution." Desalination **376**: 117-129.
495 Bouchrit, R., A. Boubakri, T. Mosbahi, A. Hafiane and S. A.-T. Bouguecha (2017). "Membrane
496 crystallization for mineral recovery from saline solution: Study case Na2SO4 crystals." Desalination
497 **412**: 1-12.

Chen, G., Y. Lu, X. Yang, R. Wang and A. G. Fane (2014). "Quantitative Study on Crystallization-Induced Scaling in High-Concentration Direct-Contact Membrane Distillation." Industrial & Engineering Chemistry Research **53**(40): 15656-15666.
Chen, G., Z. Wang, L. D. Nghiem, X.-M. Li, M. Xie, B. Zhao, M. Zhang, J. Song and T. He (2015). "Treatment of shale gas drilling flowback fluids (SGDFs) by forward osmosis: Membrane fouling and mitigation." Desalination.
Chen, Y., M. Tian, X. Li, Y. Wang, A. K. An, J. Fang and T. He (2017). "Anti-wetting behavior of negatively charged superhydrophobic PVDF membranes in direct contact membrane distillation of emulsified wastewaters." Journal of Membrane Science **535**: 230-238.
Chen, Y., R. Zheng, J. Wang, Y. Liu, Y. Wang, X.-M. Li and T. He (2017). "Laminated PTFE membranes to enhance the performance in direct contact membrane distillation for high salinity solution." Desalination **424**: 140-148.
Choi, C.-H., U. Ulmanella, J. Kim, C.-M. Ho and C.-J. Kim (2006). "Effective slip and friction reduction in nanograted superhydrophobic microchannels." Physics of Fluids **18**(8): 087105.
Choi, J., Y. Choi, Y. Jang, Y. Shin and S. Lee (2017). "Effect of aeration on CaSO4 scaling in membrane distillation process." Desalination and Water Treatment **90**: 7-15.
Choi, Y., G. Naidu, S. Jeong, S. Lee and S. Vigneswaran (2018). "Effect of chemical and physical factors on the crystallization of calcium sulfate in seawater reverse osmosis brine." Desalination **426**: 78-87.
Cottin-Bizonne, C., J. L. Barrat, L. Bocquet and E. Charlaix (2003). "Low-friction flows of liquid at nanopatterned interfaces." Nat Mater **2**(4): 237-240.
Çulfaz, P. Z., M. Haddad, M. Wessling and R. G. H. Lammertink (2011). "Fouling behavior of microstructured hollow fibers in cross-flow filtrations: Critical flux determination and direct visual observation of particle deposition." Journal of Membrane Science **372**(1–2): 210-218.
Çulfaz, P. Z., E. Rolevink, C. van Rijn, R. G. H. Lammertink and M. Wessling (2010). "Microstructured hollow fibers for ultrafiltration." Journal of Membrane Science **347**(1–2): 32-41.
Çulfaz, P. Z., M. Wessling and R. G. H. Lammertink (2011). "Hollow fiber ultrafiltration membranes with microstructured inner skin." Journal of Membrane Science **369**(1–2): 221-227.
Daniello, R. J., N. E. Waterhouse and J. P. Rothstein (2009). "Drag reduction in turbulent flows over superhydrophobic surfaces." Physics of Fluids **21**(8): 085103.
Deshmukh, A., C. Boo, V. Karanikola, S. Lin, A. P. Straub, T. Tong, D. M. Warsinger and M. Elimelech (2018). "Membrane Distillation at the Water-Energy Nexus: Limits, Opportunities, and Challenges." Energy & Environmental Science.
Duong, H. C., F. I. Hai, A. Al-Jubainawi, Z. Ma, T. He and L. D. Nghiem (2017). "Liquid desiccant lithium chloride regeneration by membrane distillation for air conditioning." Separation and Purification Technology **177**: 121-128.
Edwie, F. and T.-S. Chung (2013). "Development of simultaneous membrane distillation-crystallization (SMDC) technology for treatment of saturated brine." Chemical Engineering Science **98**: 160-172.
ElSherbiny, I. M. A., A. S. G. Khalil and M. Ulbricht (2017). "Surface micro-patterning as a promising platform towards novel polyamide thin-film composite membranes of superior performance." Journal of Membrane Science **529**: 11-22.
Eykens, L., K. De Sitter, C. Dotremont, L. Pinoy and B. Van der Bruggen (2017). "Membrane synthesis for membrane distillation: A review." Separation and Purification Technology **182**: 36-51.

Eykens, L., I. Hitsov, K. De Sitter, C. Dotremont, L. Pinoy, I. Nopens and B. Van der Bruggen (2016). "Influence of membrane thickness and process conditions on direct contact membrane distillation at different salinities." Journal of Membrane Science **498**: 353-364.
Fortunato, L., Y. Jang, J.-G. Lee, S. Jeong, S. Lee, T. Leiknes and N. Ghaffour (2018). "Fouling development in direct contact membrane distillation: Non-invasive monitoring and destructive analysis." Water Research **132**: 34-41.
Gençal, Y., E. N. Durmaz and P. Z. Çulfaz-Emecen (2015). "Preparation of patterned microfiltration membranes and their performance in crossflow yeast filtration." Journal of Membrane Science **476**: 224-233.
Godoy, A. A., L. B. d. Carvalho, F. Kummrow and P. A. Z. Pamplin (2017). "Sodium chloride as a reference substance for the three growth endpoints used in the Lemna minor L.(1753) test." Revista Ambiente & Água **12**(1): 8-16.
Granick, S., Y. Zhu and H. Lee (2003). "Slippery questions about complex fluids flowing past solids." Nature Materials **2**: 221-227.
Gryta, M. (2002). "CONCENTRATION OF NaCl SOLUTION BY MEMBRANE DISTILLATION INTEGRATED WITH CRYSTALLIZATION." Separation Science and Technology **37**(15): 3535-3558.
Gryta, M. (2002). "Direct contact membrane distillation with crystallization applied to NaCl solutions." CHEMICAL PAPERS-SLOVAK ACADEMY OF SCIENCES **56**(1): 14-19.
Gryta, M. (2008). "Fouling in direct contact membrane distillation process." Journal of Membrane Science **325**(1): 383-394.
Gryta, M. (2010). "Desalination of thermally softened water by membrane distillation process." Desalination **257**(1): 30-35.
Gryta, M. (2011). "The influence of magnetic water treatment on CaCO3 scale formation in membrane distillation process." Separation and Purification Technology **80**(2): 293-299.
Gryta, M. (2016). "Degradation of Polypropylene Membranes Applied in Membrane Distillation Crystallizer." Crystals **6**(4).
Haase, A. S., J. A. Wood, R. G. H. Lammertink and J. H. Snoeijer (2016). "Why bumpy is better: The role of the dissipation distribution in slip flow over a bubble mattress." Physical Review Fluids **1**(5).
Hashino, M., T. Katagiri, N. Kubota, Y. Ohmukai, T. Maruyama and H. Matsuyama (2011). "Effect of surface roughness of hollow fiber membranes with gear-shaped structure on membrane fouling by sodium alginate." Journal of Membrane Science **366**(1–2): 389-397.
He, F., J. Gilron and K. K. Sirkar (2013). "High water recovery in direct contact membrane distillation using a series of cascades." Desalination **323**: 48-54.
He, F., K. K. Sirkar and J. Gilron (2009). "Effects of antiscalants to mitigate membrane scaling by direct contact membrane distillation." Journal of Membrane Science **345**(1): 53-58.
He, F., K. K. Sirkar and J. Gilron (2009). "Studies on scaling of membranes in desalination by direct contact membrane distillation: CaCO3 and mixed CaCO3/CaSO4 systems." Chemical Engineering Science **64**(8): 1844-1859.
He, T., M. H. V. Mulder and M. Wessling (2003). "Preparation of porous hollow fiber membranes with a triple-orifice spinneret." Journal of Applied Polymer Science **87**(13): 2151-2157.
Hickenbottom, K. L. and T. Y. Cath (2014). "Sustainable operation of membrane distillation for enhancement of mineral recovery from hypersaline solutions." Journal of Membrane Science **454**: 426-435.

Jamshidi Gohari, R., W. J. Lau, T. Matsuura and A. F. Ismail (2013). "Effect of surface pattern formation on membrane fouling and its control in phase inversion process." Journal of Membrane Science **446**: 326-331.
Jentzsch, P. V., V. Ciobotă, B. Kampe, P. Rösch and J. Popp (2011). "Origin of salt mixtures and mixed salts in atmospheric particulate matter." Journal of Raman Spectroscopy **43**(4): 514-519.
Ji, X., E. Curcio, S. Al Obaidani, G. Di Profio, E. Fontananova and E. Drioli (2010). "Membrane distillation-crystallization of seawater reverse osmosis brines." Separation and Purification Technology **71**(1): 76-82.
Ji, Y., X.-M. Li, Y. Yin, Y.-Y. Zhang, Z.-W. Wang and T. He (2010). "Morphological control and cross-flow filtration of microfiltration membranes prepared via a sacrificial-layer approach." Journal of Membrane Science **353**(1-2): 159-168.
Jiang, X., L. Tuo, D. Lu, B. Hou, W. Chen and G. He (2017). "Progress in membrane distillation crystallization: Process models, crystallization control and innovative applications." Frontiers of Chemical Science and Engineering **11**(4): 647-662.
Julian, H., Y. Ye, H. Li and V. Chen (2018). "Scaling mitigation in submerged vacuum membrane distillation and crystallization (VMDC) with periodic air-backwash." Journal of Membrane Science **547**: 19-33.
Jung, S. Y., Y.-J. Won, J. H. Jang, J. H. Yoo, K. H. Ahn and C.-H. Lee (2015). "Particle deposition on the patterned membrane surface: Simulation and experiments." Desalination **370**: 17-24.
Junghyun, K., K. Heejung, L. Seockheon, L. Sangho and H. Seungkwan (2017). "Membrane distillation (MD) integrated with crystallization (MDC) for shale gas produced water (SGPW) treatmentjournal." Desalination **403**: 172-178.
Kharraz, J. A., M. R. Bilad and H. A. Arafat (2015). "Flux stabilization in membrane distillation desalination of seawater and brine using corrugated PVDF membranes." Journal of Membrane Science **495**: 404-414.
Kim, J., J. Kim and S. Hong (2018). "Recovery of water and minerals from shale gas produced water by membrane distillation crystallization." Water research **129**: 447-459.
Kim, J. U., S. Lee and T.-i. Kim (2016). "Recent Advances in Unconventional Lithography for Challenging 3D Hierarchical Structures and Their Applications." Journal of Nanomaterials.
Kim, P., M. J. Kreder, J. Alvarenga and J. Aizenberg (2013). "Hierarchical or Not? Effect of the Length Scale and Hierarchy of the Surface Roughness on Omniphobicity of Lubricant-Infused Substrates." Nano Letters **13**(4): 1793-1799.
Kim, P., T.-S. Wong, J. Alvarenga, M. J. Kreder, W. E. Adorno-Martinez and J. Aizenberg (2012). "Liquid-Infused Nanostructured Surfaces with Extreme Anti-Ice and Anti-Frost Performance." ACS Nano **6**(8): 6569-6577.
Latorre, M. (2005). "Environmental impact of brine disposal on Posidonia seagrasses." Desalination **182**(1): 517-524.
Lee, C., C. H. Choi and C.-J. Kim (2016). "Superhydrophobic drag reduction in laminar flows: a critical review." Exp. Fluids **57-176**.
Lee, E.-J., A. K. An, T. He, Y. C. Woo and H. K. Shon (2016). "Electrospun nanofiber membranes incorporating fluorosilane-coated TiO2 nanocomposite for direct contact membrane distillation." Journal of Membrane Science **520**: 145-154.
Lee, J.-G., Y. Jang, L. Fortunato, S. Jeong, S. Lee, T. Leiknes and N. Ghaffour (2018). "An advanced online monitoring approach to study the scaling behavior in direct contact membrane distillation."

630 Journal of Membrane Science **546**: 50-60.
631 Lee, J., C. Boo, W. H. Ryu, A. D. Taylor and M. Elimelech (2016). "Development of Omniphobic
632 Desalination Membranes Using a Charged Electrospun Nanofiber Scaffold." ACS Appl Mater
633 Interfaces **8**(17): 11154-11161.
634 Lee, Y. K., Y.-J. Won, J. H. Yoo, K. H. Ahn and C.-H. Lee (2013). "Flow analysis and fouling on the
635 patterned membrane surface." Journal of Membrane Science **427**: 320-325.
636 Li, H., H. Wang, Q. Liu, Y. Tan, N. Jiang and Y. Lin (2016). "Evaporation process for treating high-
637 salinity industrial wastewater at low temperatures and ambient pressure." Desalination and Water
638 Treatment **57**(56): 27048-27060.
639 Li, X.-M., T. He, M. Crego-Calama and D. N. Reinhoudt (2008). "Conversion of a Metastable
640 Superhydrophobic Surface to an Ultraphobic Surface." Langmuir **24**(15): 8008-8012.
641 Li, X.-M., Y. Ji, Y. Yin, Y.-Y. Zhang, Y. Wang and T. He (2010). "Origin of delamination/adhesion in
642 polyetherimide/polysulfone co-cast membranes." Journal of Membrane Science **352**(1-2): 173-179.
643 Li, X.-M., D. Reinhoudt and M. Crego-Calama (2007). "What do we need for a superhydrophobic
644 surface? A review on the recent progress in the preparation of superhydrophobic surfaces." Chemical
645 Society Reviews **36**(8): 1350-1368.
646 Li, X. M., Y. Ji, T. He and M. Wessling (2008). "A sacrificial-layer approach to prepare
647 microfiltration membranes." Journal of Membrane Science **320**(1-2): 1-7.
648 Lin, S., S. Nejati, C. Boo, Y. Hu, C. O. Osuji and M. Elimelech (2014). "Omniphobic Membrane for
649 Robust Membrane Distillation." Environmental Science & Technology Letters **1**(11): 443-447.
650 Martínez-Díez, L. and M. I. Vázquez-González (1999). "Temperature and concentration polarization
651 in membrane distillation of aqueous salt solutions." Journal of Membrane Science **156**(2): 265-273.
652 Maruf, S. H., A. R. Greenberg and Y. Ding (2016). "Influence of substrate processing and interfacial
653 polymerization conditions on the surface topography and permselective properties of surface-
654 patterned thin-film composite membranes." Journal of Membrane Science **512**: 50-60.
655 Meng, S., J. Mansouri, Y. Ye and V. Chen (2014). "Effect of templating agents on the properties and
656 membrane distillation performance of TiO2-coated PVDF membranes." Journal of Membrane
657 Science **450**: 48-59.
658 Meng, S., Y. Ye, J. Mansouri and V. Chen (2014). "Fouling and crystallisation behaviour of
659 superhydrophobic nano-composite PVDF membranes in direct contact membrane distillation."
660 Journal of Membrane Science **463**: 102-112.
661 Meng, S., Y. Ye, J. Mansouri and V. Chen (2015). "Crystallization behavior of salts during membrane
662 distillation with hydrophobic and superhydrophobic capillary membranes." Journal of Membrane
663 Science **473**: 165-176.
664 Naidu, G., S. Jeong and S. Vigneswaran (2014). "Influence of feed/permeate velocity on scaling
665 development in a direct contact membrane distillation." Separation and Purification Technology **125**:
666 291-300.
667 Naidu, G., X. Zhong and S. Vigneswaran (2018). "Comparison of membrane distillation and freeze
668 crystallizer as alternatives for reverse osmosis concentrate treatment." Desalination **427**: 10-18.
669 Nariyoshi, Y. N., C. E. Pantoja and M. M. Seckler (2016). "Evaluation of sodium chloride
670 crystallization in membrane distillation crystallization applied to water desalination." Brazilian
671 Journal of Chemical Engineering **33**(3): 675-690.
672 Nejati, S., C. Boo, C. O. Osuji and M. Elimelech (2015). "Engineering flat sheet microporous PVDF
673 films for membrane distillation." Journal of Membrane Science **492**: 355-363.

Nghiem, L. D., F. Hildinger, F. I. Hai and T. Cath (2011). "Treatment of saline aqueous solutions using direct contact membrane distillation." Desalination and Water Treatment **32**(1-3): 234-241.
Ramezanianpour, M. and M. Sivakumar (2014). "An analytical flux decline model for membrane distillation." Desalination **345**: 1-12.
Razmjou, A., E. Arifin, G. Dong, J. Mansouri and V. Chen (2012). "Superhydrophobic modification of TiO2 nanocomposite PVDF membranes for applications in membrane distillation." Journal of Membrane Science **415**: 850-863.
Ren, L.-F., F. Xia, V. Chen, J. Shao, R. Chen and Y. He (2017). "TiO2-FTCS modified superhydrophobic PVDF electrospun nanofibrous membrane for desalination by direct contact membrane distillation." Desalination **423**: 1-11.
Schofield, R. W., A. G. Fane and C. J. D. Fell (1987). "Heat and mass transfer in membrane distillation." Journal of Membrane Science **33**(3): 299-313.
Shannon, M. A., P. W. Bohn, M. Elimelech, J. G. Georgiadis, B. J. Mariñas and A. M. Mayes (2008). "Science and technology for water purification in the coming decades." Nature **452**: 301-310.
Shin, D. H., J. B. Park, Y. J. Kim, S. J. Kim, J. H. Kang, B. Lee, S. P. Cho, B. H. Hong and K. S. Novoselov (2015). "Growth dynamics and gas transport mechanism of nanobubbles in graphene liquid cells." Nature Communications **6**.
Shin, Y. and J. Sohn (2016). "Mechanisms for scale formation in simultaneous membrane distillation crystallization: Effect of flow rate." Journal of Industrial and Engineering Chemistry **35**: 318-324.
Tang, L., A. Iddya, X. Zhu, A. V. Dudchenko, W. Duan, C. Turchi, J. Vanneste, T. Y. Cath and D. Jassby (2017). "Enhanced Flux and Electrochemical Cleaning of Silicate Scaling on Carbon Nanotube-Coated Membrane Distillation Membranes Treating Geothermal Brines." Acs Applied Materials & Interfaces **9**(44): 38594-38605.
Tian, M., X. Li, Y. Yin, T. He and J. Liu (2015). "Preparaton of superhydrophobic membranes and their application in membrane distillation." Progress in Chemstry **27**(8): 1033-1041.
Tian, M., Y. Yin, C. Yang, B. Zhao, J. Song, J. Liu, X.-M. Li and T. He (2015). "CF4 plasma modified highly interconnective porous polysulfone membranes for direct contact membrane distillation (DCMD)." Desalination **369**: 105-114.
Tijing, L. D., Y. C. Woo, J.-S. Choi, S. Lee, S.-H. Kim and H. K. Shon (2015). "Fouling and its control in membrane distillation-A review." Journal of Membrane Science **475**: 215-244.
Tijing, L. D., Y. C. Woo, W.-G. Shim, T. He, J.-S. Choi, S.-H. Kim and H. K. Shon (2016). "Superhydrophobic nanofiber membrane containing carbon nanotubes for high-performance direct contact membrane distillation." Journal of Membrane Science **502**: 158-170.
Truesdell, R., A. Mammoli, P. Vorobieff, F. van Swol and C. J. Brinker (2006). "Drag reduction on a patterned superhydrophobic surface." Phys Rev Lett **97**(4): 044504.
Tun, C. M., A. G. Fane, J. T. Matheickal and R. Sheikholeslami (2005). "Membrane distillation crystallization of concentrated salts—flux and crystal formation." Journal of Membrane Science **257**(1): 144-155.
Tyree, C. A., V. M. Hellion, O. A. Alexandrova and J. O. Allen (2007). "Foam droplets generated from natural and artificial seawaters." Journal of Geophysical Research: Atmospheres **112**(D12).
Tyrrell, J. W. G. and P. Attard (2001). "Images of Nanobubbles on Hydrophobic Surfaces and Their Interactions." Physical Review Letters **87**(17): 176104.
Wang, Z. X., D. Y. Hou and S. H. Lin (2016). "Composite Membrane with Underwater-Oleophobic Surface for Anti-Oil-Fouling Membrane Distillation." Environmental Science & Technology **50**(7):

718 3866-3874.
719 Wang, Z. X., J. Jin, D. Y. Hou and S. H. Lin (2016). "Tailoring surface charge and wetting property
720 for robust oil-fouling mitigation in membrane distillation." Journal of Membrane Science **516**: 113-
721 122.
722 Warsinger, D. M., A. Servi, S. Van Belleghem, J. Gonzalez, J. Swaminathan, J. Kharraz, H. W.
723 Chung, H. A. Arafat, K. K. Gleason and J. H. V. Lienhard (2016). "Combining air recharging and
724 membrane superhydrophobicity for fouling prevention in membrane distillation." Journal of
725 Membrane Science **505**: 241-252.
726 Wei, X., B. Zhao, X.-M. Li, Z. Wang, B.-Q. He, T. He and B. Jiang (2012). "CF4 plasma surface
727 modification of asymmetric hydrophilic polyethersulfone membranes for direct contact membrane
728 distillation." Journal of Membrane Science **407-408**: 164-175.
729 Wilson, P. W., W. Lu, H. Xu, P. Kim, M. J. Kreder, J. Alvarenga and J. Aizenberg (2013). "Inhibition
730 of ice nucleation by slippery liquid-infused porous surfaces (SLIPS)." Physical Chemistry Chemical
731 Physics **15**(2): 581-585.
732 Won, Y.-J., S.-Y. Jung, J.-H. Jang, J.-W. Lee, H.-R. Chae, D.-C. Choi, K. Hyun Ahn, C.-H. Lee and
733 P.-K. Park (2016). "Correlation of membrane fouling with topography of patterned membranes for
734 water treatment." Journal of Membrane Science **498**: 14-19.
735 Won, Y. J., J. Lee, D. C. Choi, H. R. Chae, I. Kim, C. H. Lee and I. C. Kim (2012). "Preparation and
736 application of patterned membranes for wastewater treatment." Environ Sci Technol **46**(20): 11021-
737 11027.
738 Xie, M., W. Luo and S. R. Gray (2017). "Surface pattern by nanoimprint for membrane fouling
739 mitigation: Design, performance and mechanisms." Water Research **124**: 238-243.
740 Xing, L., J. Song, Z. Li, J. Liu, T. Huang, P. Dou, Y. Chen, X.-M. Li and T. He (2016). "Solvent
741 stable nanoporous poly (ethylene-co-vinyl alcohol) barrier membranes for liquid-liquid extraction of
742 lithium from a salt lake brine." Journal of Membrane Science **520**: 596-606.
743 Xue Mei Li, M. C. C. (2007). "The rough with the smooth." Chemical Science **4**: C75.
744 Yang, C., X.-M. Li, J. Gilron, D.-f. Kong, Y. Yin, Y. Oren, C. Linder and T. He (2014). "CF4 plasma-
745 modified superhydrophobic PVDF membranes for direct contact membrane distillation." Journal of
746 Membrane Science **456**: 155-161.
747 Yang, C., M. Tian, Y. Xie, X.-M. Li, B. Zhao, T. He and J. Liu (2015). "Effective evaporation of CF4
748 plasma modified PVDF membranes in direct contact membrane distillation." Journal of Membrane
749 Science **482**: 25-32.
750 Yun, Y., R. Ma, W. Zhang, A. G. Fane and J. Li (2006). "Direct contact membrane distillation
751 mechanism for high concentration NaCl solutions." Desalination **188**(1): 251-262.
752 Zou, T., X. Dong, G. Kang, M. Zhou, M. Li and Y. Cao (2018). "Fouling behavior and scaling
753 mitigation strategy of CaSO4 in submerged vacuum membrane distillation." Desalination **425**: 86-
754 93.

755